SCIENCE CHINA
Earth Sciences

• RESEARCH PAPER •

October 2014 Vol.57 No.10: 2397–2407
doi: 10.1007/s11430-014-4890-8

The influence of rainfall on PR radar measurement of ocean surface wind speed and its calibration

LIU Peng[1,2,3], GU XingFa[1,2*], YU Tao[1,2], LI Juan[1,2] & DONG Wen[1,2]

[1] *State Key Laboratory of Remote Sensing Science, Institute of Remote Sensing and Digital Earth, Chinese Academy of Sciences, Beijing 100101, China;*
[2] *Demonstration Centre for Spaceborne Remote Sensing National Space Administration, Beijing 100101, China;*
[3] *University of Chinese Academy of Sciences, Beijing 100049, China*

Received July 31, 2013; accepted November 18, 2013; published online August 7, 2014

Rain can significantly degrade the wind vector retrieval from Precipitation Radar (PR) by three mechanisms, namely, two-way rain attenuation, rain volume-backscattering, and ocean surface roughening from the rain splash effect. Here we first derive the radar equation for PR in rainy conditions. Then we use the rain attenuation model for Ku band, volume backscatter model for spherical raindrops and PR–TMI (TRMM Microwave Imager, TMI) matchup datasets from June to August in 2010 to solve the radar equation, and quantitatively analyze the influence of rainfall on PR radar measurement of ocean surface wind speed. Our results show that the significant effect of rain on radar signal is dominated by two-way rain attenuation and rain splash effect, and the effect of rain volume-backscattering is relatively the weakest, which can even be neglected in rain-weak conditions. Moreover, both the two-way rain attenuation and rain splash effect increase with the increasing of integration rain rate and incident angle. Last, we combine volume-backscattering effect and splash effect into a simple phenomenological model for rain calibration and select three typhoon cases from June to August in 2012 to verify the accuracy of this model. Before calibration, the mean difference and mean square error (MSE) between PR-observed σ^0 and wind-induced σ^0 are about 2.95 dB and 3.10 dB respectively. However, after calibration, the mean difference and MSE are reduced to 0.64 dB and 1.61 dB respectively. The model yields an accurate calibration for PR near-nadir normalized radar cross section (NRCS) in rainy conditions.

Precipitation Radar, two-way path attenuation, volume-backscattering, splash effect, radiative transfer model in rainy conditions

Citation: Liu P, Gu X F, Yu T, et al. 2014. The influence of rainfall on PR radar measurement of ocean surface wind speed and its calibration. Science China: Earth Sciences, 57: 2397−2407, doi: 10.1007/s11430-014-4890-8

Ocean surface wind is the main driving factor for ocean circulation, which modulates the exchange of vapor flux, heat flux, carbon dioxide flux, and other gases. Accurate measurement of the ocean surface wind can be beneficial for understanding the global climate change. Over the past several years, microwave remote sensing has brought considerable breakthroughs to the ocean sciences by providing large-scale synoptic views of the surface wind field over global ocean because of their abilities to survey the earth in the way of all day, all weather and all regions. And the ocean surface wind measurements from microwave remote sensing are widely used for numerical weather prediction, tropical cyclone monitoring and so on (Graf, 1998; Quilfen, 1998).

At present, there are two kinds of active radar system which operate at Ku band and can retrieve ocean surface wind accurately, known as the QuikSCAT and the Precipitation Radar (PR) respectively. QuikSCAT and PR have

*Corresponding author (email: gis_lp123@163.com)

very different scan geometries and spatial resolutions. The QuikSCAT is a conically scanning radar scatterometer that operates at large incidence, transmitting and receiving cross-polarization radar signals described by Bragg-scattering mechanism. The PR radar operates at small incidence, transmitting and receiving horizontally polarized radar signal described by quasi-specular scattering mechanism. Both instrumental wind retrievals are based on the relationship between the normalized radar cross section (NRCS, σ^o) of the ocean surface and wind speed, known as Ku-band geophysical model function (GMF). Previous investigations showed that both instruments can retrieve ocean wind speed accurately under neutral atmospheric stability conditions; however, the quality of QuikSCAT or PR retrieved winds is very poor in rainy conditions, especially in storm regions. The main reason is the effect of rain on radar signal and can be summarized as follows: firstly, the radar signal is attenuated and scattered by rainfall, denoted as two-way rain attenuation. Secondly, when scattered by rainfall, a few parts of scattering signal return to radar system, denoted as volume-scattering. Lastly, rain striking the surface perturbs the wind-wave field and causes additional scattering from rain-induced surface features, denoted as the splash effect.

Researchers have extensively studied the impact of rainfall on QuikSCAT signal and proposed a series of rain calibration models (Donneley et al., 1999; Yueh et al., 2001, 2003; Li et al., 2004; Nielsen et al., 2007; Laupattarakasem et al., 2011). And some of these models are still in a state of developing and updating. Since the PR was designed specifically for measuring the atmospheric moisture and the atmosphere precipitation profiles over the tropical ocean, but for ocean surface wind field, researchers always ignored the impact of rainfall on PR measurement of ocean surface wind. The spatial and temporal resolution of PR measurements is superior to that of the QuikSCAT. Furthermore, because the observation areas of PR are concentrated mainly in the tropical ocean and land, where are rich in precipitation, the PR signal that returns from ocean surface is more susceptible to rainfall. In recent years, with the invalidation of QuikSCAT and the advantage of PR observations over tropical marine areas, the impact of rainfall on PR measurement of ocean surface wind draws more attention from scientists. Meneghin (2000) first used the surface reference technique (SRT) to estimate the PR signal path-integrated attenuation due to rainfall. This technique assumes uniform ocean surface backscattering background at precipitation scale and attributes the difference in measured surface backscattering cross sections inside and outside of storms to path-integrated attenuation. But the results in Meneghin's paper did not analyze the rain volume backscatter and ocean surface roughening from the splash effect quantitatively. Li (2001) used a surface wind model-based method to estimate rain-induced PR path attenuation over ocean. Although there is excellent agreement between wind fields retrieved from TRMM PR and TMI data in rainy conditions, the result has the same problem as in Meneghin's research. Moreover, several other experimental rain correction models have been published that show promise for providing improved ocean surface winds in rainy conditions (Li et al., 2007; Shang et al., 2009).

By studying the above-mentioned literatures, we found that previous studies failed to adequately analyze how rain affects the PR echo signal, especially the rain splash effect. That is due partially to the lack of effective means to describe the state of ocean surface roughness caused by rain splash effect. Bliven et al. (1997) and Craeye et al. (1997) used the a ring-wave spectral model to depict the additional roughness caused by rain on a wind driven surface based on laboratory wind-wave tank data; however, the results were only suitable for the case of medium or large incidence. As we know, PR operates at small incidence (0°–18°) and the scattering mechanism between electromagnetic wave and ocean surface in small incidence departs from medium or large incidence, so the wind-wave spectral model proposed by Bliven et al. (1997) and Craeye et al. (1997) is not suitable for our research. In fact, the total PR echo energy scattered from ocean surface in rainy conditions is the result of interaction of two-way rain attenuation, rain volume backscatter, rain splash effect and ocean surface wind. Therefore, if the values of other components can be evaluated accurately, the splash effect can be estimated indirectly by solving the PR radar equation in rainy conditions.

First, we develop the radar equation for PR in rainy condition. Then we use the rain attenuation model for Ku band, volume backscatter model for spherical raindrops and PR-TMI matchup datasets from June to August in 2010 to solve the radar equation, and quantitatively analyze the influence of rainfall on PR radar measurement of ocean surface wind speed. Lastly, we propose a rain calibration model for PR and select three typhoon observations that occurred from June to August in 2012 to verify the accuracy of this model. Our research can provide a theoretical basis for PR in typhoon-monitoring, and would be beneficial for expanding the business applications of PR over the tropical ocean.

1 Radar equation in rainy condition

PR is an active radar system, and the relationship of PR radar system, ocean surface and echo signal can be described by radar equation, and given by

$$P_r = \frac{P_t G^2 \lambda^2}{(4\pi)^3 R^4} \sigma^0, \tag{1}$$

where P_r and P_t are respectively total radar received power and transmitted powers. The coefficients G, λ, and R are antenna gain, the length of incident electromagnetic wave,

and the distance between radar antenna and ocean surface respectively. And the σ^0 is the Normalized Radar Cross Section (NRCS) of ocean surface which equals σ^0_{wind} caused by ocean surface wind:

$$P_r = \frac{P_t G^2 \lambda^2}{(4\pi)^3 R^4} \sigma^0_{\text{wind}}. \quad (2)$$

Rain is a phenomenon with various falling rain particles. When radar signal passes through the precipitation layers, raindrops not only absorb the electromagnetic energy, but also scatter the electromagnetic energy. And these two effects cause the two-way attenuation for radar signal along the round-trip propagation path, denoted as *K*. Moreover, a few parts of the scattered electromagnetic wave will return to the radar system along the incident direction, and this will increase the radar detection power known as volume-backscattering NRCS, denoted as σ^0_r. Taking into account the two-way rain attenuation and rain volume-backscattering, we get

$$P_r = \frac{P_t G^2 \lambda^2}{(4\pi)^3 R^4} \left[\sigma^0_{\text{wind}} \cdot K + \sigma^0_r \right]. \quad (3)$$

When raindrops fall into the ocean surface, rain striking the water creates rings, stalks, and crowns to perturb the short gravity wave field and cause additional scattering from rain-induced surface features known as the rain splash effect, denoted as σ^0_{surf} ($\sigma^0_{\text{surf}} \geqslant 0$) (Manton et al., 1973; Green et al., 1979; Nystuen et al., 1990; Yang et al., 1997). Therefore, the sea surface roughness is a result of the interaction of wind-wave and rain-induced surface features. And both features can be cumulative (David et al., 2004). Furthermore, additional scattering signal caused by the splash effect is also subjected to the two-way attenuation effect when it returns to radar system, so the additional scattering signal which radar can detect changes into $-\sigma^0_{\text{surf}} \cdot K$ practically. In view of the splash effect, the radar equation can be written as

$$P_r = \frac{P_t G^2 \lambda^2}{(4\pi)^3 R^4} \left[\sigma^0_{\text{wind}} \cdot K + \sigma^0_{\text{surf}} \cdot K + \sigma^0_r \right]. \quad (4)$$

But eq. (4) is only suitable for radar system that operates at medium or large incidence (>30°). For medium or large incidence, the radar signal is dominated by Bragg resonance diffraction. With the increasing of rain intensity, the sea surface gets rougher, and radar echo signal power gets stronger. Therefore, the splash effect is to increase the radar-observed signal power scattered actually by ocean surface. However, the PR operates at small incidence (0°–18°). For small incidence, the radar signal is dominated by quasi-specular scattering. A completely flat sea surface or surface with low roughness leads to the maximum scattering signal. With the perturbation of rainfall, sear surface gets rougher, and more PR signals will be scattered along other directions which depart from the incident direction. In other words, the perturbation of rain on sea surface roughness is to reduce the radar-observed signal power at low incidence, and that is contrary to the radar systems that operate at medium or large incidence. So, given the PR space observational characteristics, the splash effect $\sigma^0_{\text{surf}} \cdot K$ changes into $-\sigma^0_{\text{surf}} \cdot K$. We thus write eq. (4) as

$$P_r = \frac{P_t G^2 \lambda^2}{(4\pi)^3 R^4} \left[\sigma^0_{\text{wind}} \cdot K - \sigma^0_{\text{surf}} \cdot K + \sigma^0_r \right]. \quad (5)$$

And the total PR signal power returns from ocean surface in rainy conditions given by

$$\sigma^0_{\text{obs}} = \left(\sigma^0_{\text{wind}} - \sigma^0_{\text{surf}} \right) \cdot K + \sigma^0_r. \quad (6)$$

In the following sections, we will solve each component of the radar equation and quantitatively analyze the influence of rainfall on PR radar measurements.

1.1 Two-way rain attenuation

The rain attenuation is considered relevant to the raindrop radius and the wavelength of electromagnetic waves, and is denoted as a function of rain rate and rain height, which, most widely used in the numerical simulation, is the rain radiative transfer model (Nielsen et al., 2007). This model was developed on the basis of the collocated datasets from QuikSCAT NRCS data and Advanced Microwave Scanning Radiometer (AMSR) rain rate data. The most prominent feature of this model is that the collocated datasets do not exit temporal matching errors. And it takes the form:

$$10 \cdot \lg(K) = -10^{\sum_{n=0}^{2} C(n) \cdot R_{\text{ir}}^n / 10}, \quad (7)$$

where *K* is the two-way path attenuation, and *C*(*n*) are the model coefficients. Their values are –0.92879, 1.0379 and –0.0151 for H polarization, and –9.0998, 1.1747 and –0.022 for V polarization. R_{ir} (dB km mm h^{-1}) is the integration rain rate, which is a sum of rain rate R_i (mm h^{-1}) of precipitation layers, and is described as a product of rain rate and rain height:

$$R_{\text{ir}} = 10 \cdot \lg\left(\int_0^{H \cdot \sec(\vartheta)} R_i \mathrm{d}r \right), \quad (8)$$

where *H* is the thickness of precipitation layers (km), and ϑ is the angle between incident wave direction and precipitation layers. According to that the thickness of precipitation layers *H* varies from locations, time, rain type, and rain rate. Consequently, *H* should be a representative of average, rather than individual, rainfall conditions and is set to 3 km (Chiu et al., 2000; Thurai et al., 2005; Nielsen et al., 2007;

Zhang L et al., 2010).

1.2 Rain volume-backscattering

For Ku band electromagnetic waves, the backscattering cross-section of individual raindrops can be described by Mie-scattering theory (Zhang P C et al., 2000; Liu L et al., 2008). In a rain volume, the particles usually are assumed to be randomly distributed and spherical within the volume, so that there are no coherent phase relationships between the fields scattered by the individual particles, thereby allowing the use of incoherent scattering theory for computing the scattering and absorption by rain particles. Moreover, the concentration of particles usually is small enough to support the assumption that shadowing of one particle by another may be ignored. From the above two assumptions, we can conclude that the total backscattering cross-section of a given volume is equal to the sum of the backscattering cross-sections of all the rain particles contained in the volume (Ulaby et al., 1981). Thus

$$\sigma_b^0 = \frac{\lambda^3}{8\pi^2}\int_0^\infty \chi^2 \xi_b(\chi)\, p(\chi)\mathrm{d}\chi, \tag{9}$$

where σ_b^0 is the total backscattering cross-section per unit volume (Np m^{-1}). χ is a dimensionless parameter and $\chi=2\pi r/\lambda$ .The coefficients r and λ are the rain radius and length of incident wave respectively. Usually, the radius of raindrops may be defined as a range (0.05–4 mm). If the radius of raindrops is larger than 4 mm, raindrops will be broken due to instability of large particles. And $\xi_b(\chi)$ is the backscattering efficiency described by Mie scattering theory:

$$\xi_b = \frac{1}{\chi^2}\left|\sum_{m=1}^{\infty}(-1)^m(2m+1)(a_m - b_m)\right|^2, \tag{10}$$

where a_m and b_m are Mie coefficients which are functions of χ and m. The coefficient m is an integer of infinity; however, m is difficult to take the case to infinity in the process of numerical calculation. When m is larger than a specific integer, the value of eq. (10) will not change. Considering computational efficiency and accuracy, m is taken to 200 here. Additionally, the formal expressions for Mie coefficients involve Bessel functions of complex argument. For computational purposes, we use an iterative procedure that was developed by Deirmendjian (Ulaby et al., 1981) for Bessel functions:

$$a_m = \frac{(A_m/n + m/\chi)\mathrm{Re}\{W_m\} - \mathrm{Re}\{W_{m-1}\}}{(A_m/n + m/\chi)W - W_{m-1}}, \tag{11}$$

$$b_m = \frac{(A_m n + m/\chi)\mathrm{Re}\{W_m\} - \mathrm{Re}\{W_{m-1}\}}{(A_m n + m/\chi)W - W_{m-1}}, \tag{12}$$

and his development leads to expressions

$$\begin{cases} W_m = ((2m-1)/\chi)W_{m-1} - W_{m-2}, \\ W_0 = \sin\chi + j\cos\chi, \\ W_{-1} = \sin\chi - j\cos\chi, \\ A_m = -1/n\chi + (1/n\chi - A_{m-1})^{-1}, \\ A_0 = \cot n\chi, \end{cases} \tag{13}$$

where n is a complex of the refractive index of rain, and is a function of relative complex permittivity ε which is calculated by Ray empirical formula ($\varepsilon = \varepsilon' - j\varepsilon''$, $n = \sqrt{\varepsilon}$) (Ray el al., 1972).

The coefficient $p(\chi)$ is the raindrop-size distribution model which is representative of number of drops of diameter per unit volume and per unit drop-diameter interval. The measurements of raindrop size distributions show large variations for the same location, rain type, and rain rate. Consequently, drop-size distribution models should be regarded as representative of average, rather than individual, rainfall conditions. The raindrop-size distribution has been determined by several investigations including M-P model, Wei-bull model and log-normal model. Among these, the most widely used in the numerical simulation for rain attenuation is the M-P distribution model owing to the calculation simplicity (Ulaby et al., 1981; Lin et al., 1981; Liu et al., 2008; Liu et al., 2010). Thus

$$p(\chi) = a\cdot\exp\left(-bR^{0.21}\chi\right), \tag{14}$$

where R is the rain rate (mm h^{-1}), and a=8000 m^{-3} mm^{-1}, b=4.1.

And then the volume backscattering cross-section from the precipitation layers in the propagation path of electromagnetic wave (Figure 1) can be computed using eq. (14):

$$\sigma_r^0 = \sigma_b^0 \cdot H \cdot \sec(\vartheta), \tag{15}$$

where, as previously defined, σ_b^0 is the total backscattering cross-section per unit volume, and H is the thickness of precipitation layers. ϑ is the angle between incident wave direction and precipitation layers. In most cases, due to the effect of curvature of the earth, the satellite orbit and the state of precipitation layers, it is difficult to determine the value of ϑ directly. According to David and Nielsen's investigations, here we assume ϑ equals θ which is the radar incidence angle (David et al., 2004; Nielsen et al., 2007).

Although the falling raindrops are not perfectly spherical, this departure from the spherical shape assumed in the computation increases with the size of the raindrop. Previous observations (Oguchi, 1964; Crane, 1971) indicate that the non-spherical particle leads to a polarization dependence of the fields scattered by the raindrop. And therefore the effects departure from perfectly spherical particles can be ignored. From a practical standpoint, eq. (15) can fully describe the backscattering of raindrops.

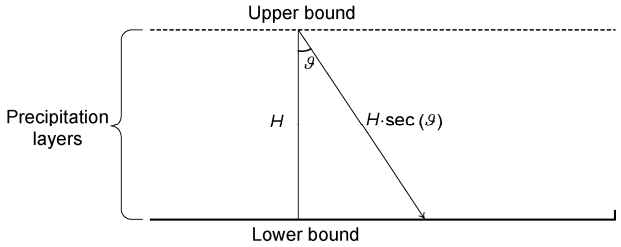

Figure 1 The illustration of raindrops passing through the precipitation layers.

1.3 Rain splash effect

Thus far, all rain-induced parameters of eq. (6) except the splash effect $-\sigma^0_{\text{surf}} \cdot K$ have been estimated. From the above-mentioned, the splash effect is often ignored by theoretical models due to a lack of understanding of its effects. However, it is very important to include the splash effect to afford the besting modeling of rain. And this can be done indirectly using the radar eq. (6), thus

$$-\sigma^0_{\text{surf}} \cdot K = \sigma^0_{\text{obs}} - \sigma^0_r - \sigma^0_{\text{wind}} \cdot K, \tag{16}$$

where $-\sigma^0_{\text{surf}} \cdot K$ is unknown, and σ^0_{wind} is the wind-induced backscatter in rain-free conditions calculated by using the GMF and TMI ocean surface wind data:

$$\sigma^0_{\text{wind}} = \text{GMF}(U_{10}, \theta), \tag{17}$$

where U_{10} is the wind speed at 10 m above sea surface, and θ is the PR incident angle. GMF is the geophysical model function and we choose the SASS-2/PR model (Li et al., 2004).

2 Data description

We calculate the parameters from eq. (6) by synergistically combining co-located data from PR and TRMM Microwave Imager (TMI) to estimate the PR-observed backscatter and attenuation from rain. Rain rate data and ocean surface wind data are provided by PR and TMI respectively.

The PR was placed on the Tropical Rainfall Measuring Mission (TRMM) satellite and operates at 13.8 GHz. The PR is the first space-borne broad-swath radar capable of measuring ocean radar backscatter at relatively low incidence angles over a significant swath width and with high spatial resolution. The full PR measurement swath is about 215 km wide, with continuous surface backscatter cross-section measurements having spatial resolution of about 4.3 km. The PR 2A21 standard product obtained from the Goddard Distributed Active Archive Center (NAAC) forms the basis for the results presented here. It contains information on ocean surface radar backscatter cross-section, total path attenuation, and integration rain rate, as well as standard quality flags and navigation and instrument geometry (e.g., incidence angle) information.

The TMI antenna scans conically at a fixed incidence angle collecting measurements from left to right over a 758.5-km swath divided into 104 low-resolution samples or 208 high-resolution samples. The TMI 1B11 standard product forms the basis for the results presented here. It contains information on ocean surface brightness temperatures. In this paper, we will use an empirical model for TMI derived by Connor and Chang (Conner et al, 2000) from collocated TMI and buoy data using the D-Matrix technique to get the sea surface ocean wind speed. The overall accuracy for this model is about 1.5 m/s and is proved to be right over the most part of tropical ocean, and we have

$$\begin{aligned} U_{20} = {} & C_0 + C_1 T_B(19V) + C_2 T_B(22V) \\ & + C_3 T_B(37V) + C_4 T_B(37V), \end{aligned} \tag{18}$$

where U_{20} is the wind speed at 20 m above the sea surface, and C_n are the model coefficients. Because PR and TMI are placed on the same satellite, we can ignore the temporal matching errors. Additionally, note that the usual reference wind is taken at 10 m above the sea surface (U_{10}), a convention which will be used throughout this paper. The TMI wind speed will be calculated by converting U_{20} to U_{10} using a classical von Karman logarithmic profile (Durden et al., 1985), described as

$$U_{10} = (u_*/0.4)\ln\left[\frac{10 \cdot \exp(0.4U_{20}/u_*)}{20}\right], \tag{19}$$

where u_* is the friction velocity.

To obtain coincident PR and TMI observations at the same resolution, a program was developed to co-locate the PR samples with the raw 10.7-GHz TMI footprint. The matchup procedure is similar to the one used by the standard TRMM that combined TMI and PR precipitation algorithm (Li et al., 2004). Furthermore, as the PR-observed σ^0 fluctuates seriously due to rainfall, platform jitter and so on, we use a 3-sigma law to rule out the abnormal data, defined as

$$\begin{cases} \left|\sigma^0 - E(\sigma^0)\right| \leqslant 3 \cdot \text{std}(\sigma^0), & \text{Keep}, \\ \left|\sigma^0 - E(\sigma^0)\right| > 3 \cdot \text{std}(\sigma^0), & \text{Exclude}, \end{cases} \tag{20}$$

where $E(\sigma^0)$ is the mean value of σ^0, and std(σ^0)is the standard deviation of σ^0. The collocation and quality control procedure were applied to the 3 months of data for the period of June to August in 2012, from which 1321978 PR-TMI match-up datasets were collected.

3 The influence of rainfall on PR signal

Given the effect of shadowing of one raindrop by another,

breaking of raindrops, and rain rate saturation of microwave brightness temperature when rain rate is larger than 50 mm h^{-1}, the rain rate data collected in this paper are limited to 50 mm h^{-1}. Figures 2–4 plot the effect of rain two-way attenuation, rain volume-backscattering, and rain splash effect versus rain intensity for different incidence angels respectively, and rain intensity R is transformed from rain rate R_i by $R=10\cdot\log10(R_i)$. Error bars reflect the mean value and mean difference of observing objects per rain intensity, and color bars reflect the number of matching data per node.

Figure 2 shows that the effect of rain two-way attenuation on PR signal is dominated by rain intensity for different incidence angles. When rain intensity is smaller than 0 dB mm h^{-1}, the value of rain two-way attenuation is very close to 1, and the effect of rain two-way attenuation can be neglected. As the rain intensity increases up to 17 dB mm h^{-1}, the effect of rain two-way attenuation becomes very strong; therefore, only 40% of PR signal power can return to radar system. Additionally, comparing the effect of rain two-way attenuation for different incidence angles, we find that the effect of rain two-way attenuation is increasing as the incidence at the same rain intensity. For example, when rain intensity equals 17 dB mm h^{-1}, the value of rain two-way attenuation is about 0.40 within 0°–4°, and about 0.37 within 15°–18°. The reason can be summarized as follows: with incidence angles increasing, the path of radar signal passing through the precipitation layers increases, and therefore, the effect of rain two-way attenuation becomes stronger.

Figure 3 plots rain volume backscattering NRCS against rain intensity and incidence angle. As the shadowing of one raindrop by another can be ignored, rain volume backscattering NRCS shows an increasing trend with rain intensity, and the value of rain volume backscattering NRCS is within a spread of 0–0.12. Additionally, the incidence dependence of rain volume backscattering NRCS is relatively weak. As the incidence angle increases, the path of radar signal passing through the precipitation layers increases, and more raindrops will scatter the PR radar signal to radar system; therefore the PR-observed signal increases. For example, when rain intensity equals 17 dB mm h^{-1}, the rain volume backscattering NRCS is about 0.097 within 0°–4°, and about 0.11 within 15°–18° .

Figure 4 plots NRCS due to the splash effect calculated by eq. (16) against the rain intensity for different incidence. Note that eq. (16) error contains not only errors in GMF but also errors associated with instrument calibration and the calculation errors. Although the rain intensity dependence of $-\sigma^0_{\text{surf}}\cdot K$ is not perfectly monotonic, we can see that $-\sigma^0_{\text{surf}}\cdot K$ decreases with the increasing of rain intensity in the main; that is to say, the splash effect is to reduce the PR signal power and this effect increases with the increasing of rain intensity. The reason is that the roughness of sea surface increases with the increasing of rain intensity, and therefore, more PR signals will be scattered along other directions which depart from the incident direction. Moreover, we find that the value of $-\sigma^0_{\text{surf}}\cdot K$ decreases with the increasing of incidence. It can be attributed to the interaction of quasi-specular scattering and Bragg scattering.

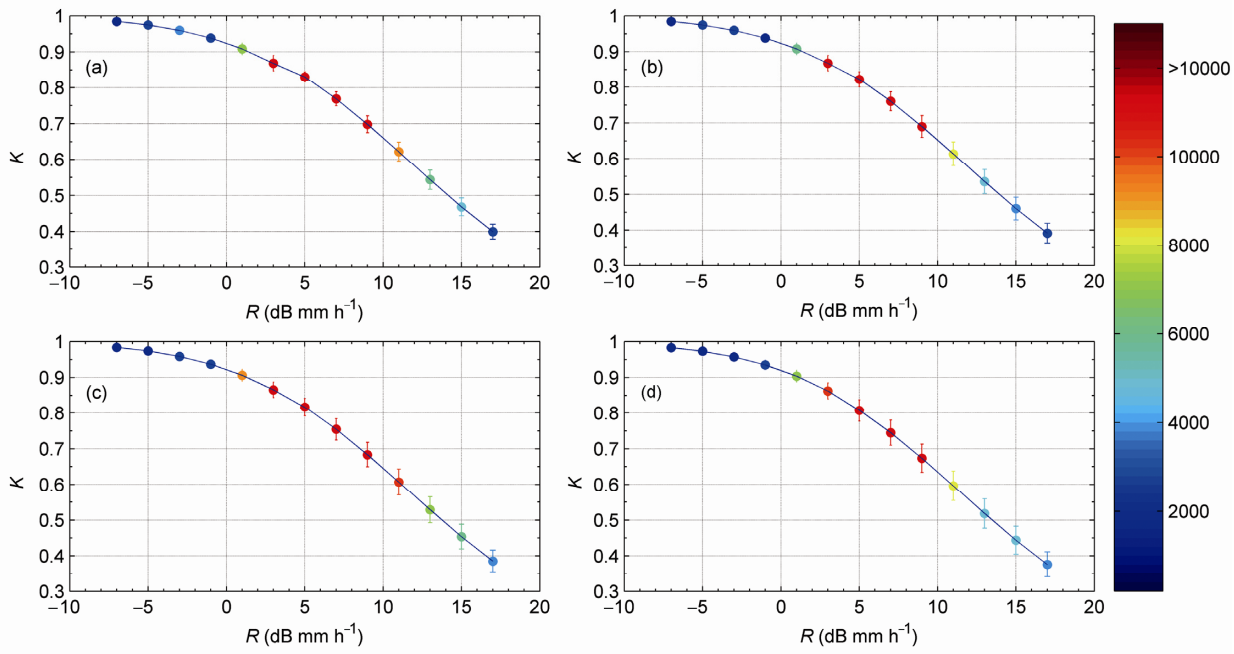

Figure 2 The relationship between rain two-way attenuation and rain intensity for different incidence angles. (a) 0°–4°; (b) 5°–9°; (c) 10°–14°; (d) 15°–18°.

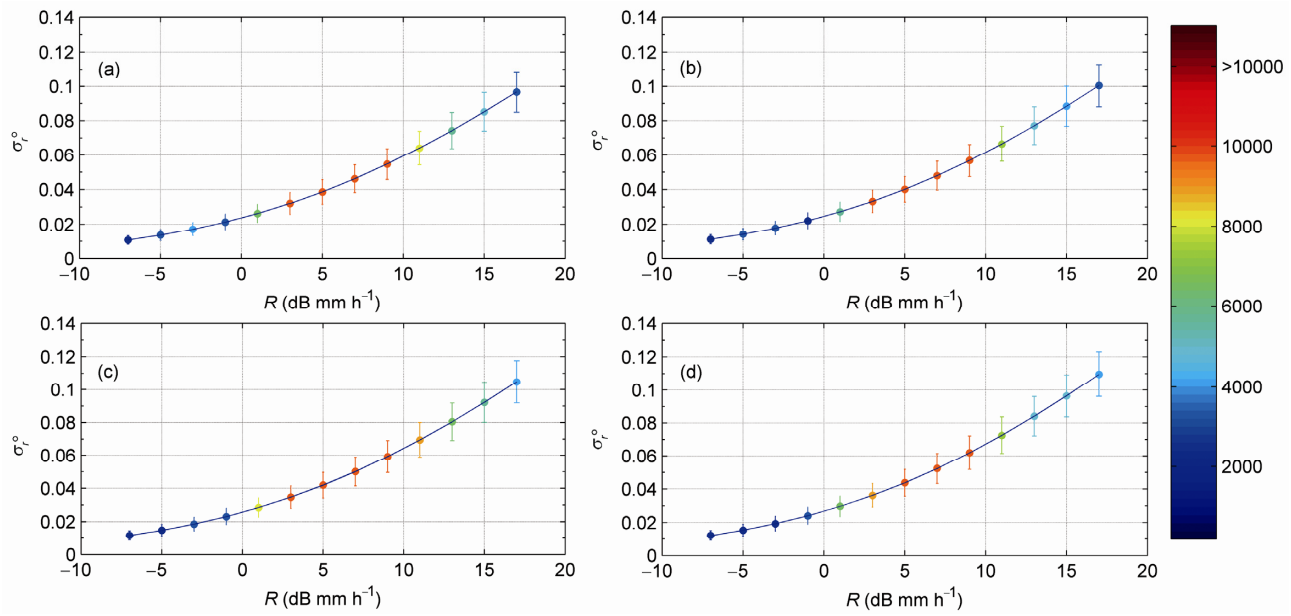

Figure 3 The relationship between rain volume-backscattering NRCS and rain intensity for different incidence angels. (a) 0°–4°; (b) 5°–9°; (c) 10°–14°; (d) 15°–18°.

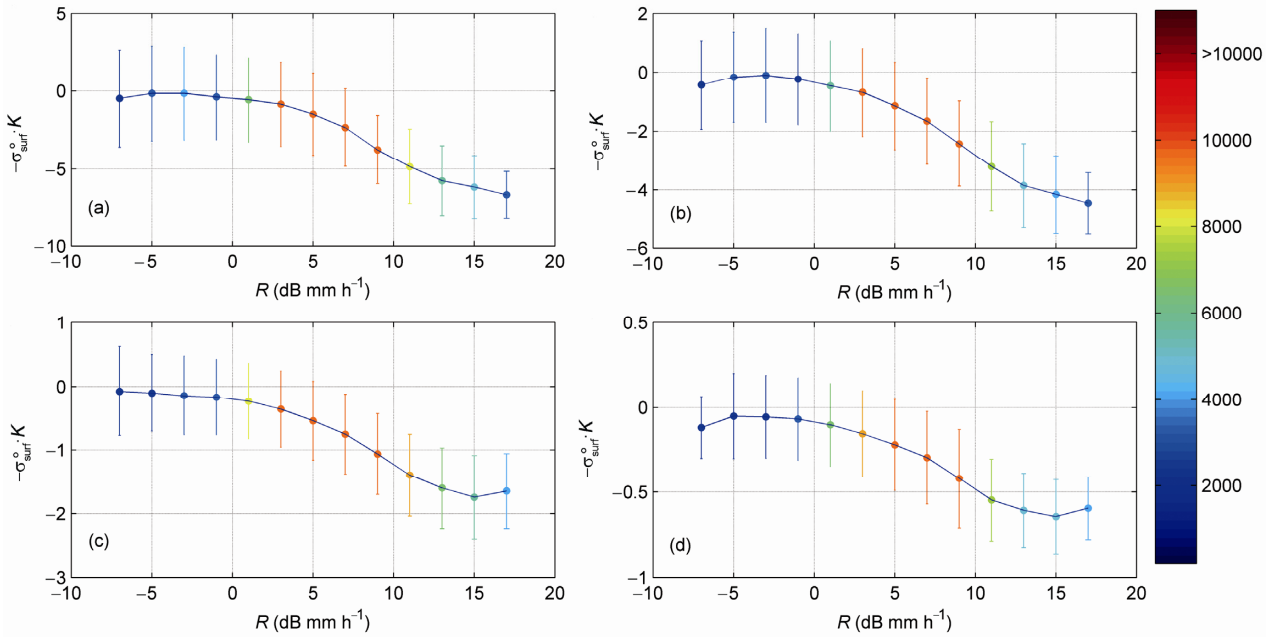

Figure 4 The relationship between NRCS due to the splash effect and rain intensity for different incidence. (a) 0°–4°; (b) 5°–9°; (c) 10°–14°; (d) 15°–18°.

4 The rain radiative transfer model

4.1 Radiative transfer model

To simplify the calculation, we introduce a new parameter σ_{eff}^0, which is a combination of σ_r^0 and $-\sigma_{\text{surf}}^0 \cdot K$, denoted as effective rain backscattering cross-section:

$$\sigma_{\text{eff}}^0 = -\sigma_{\text{surf}}^0 \cdot K + \sigma_r^0. \tag{21}$$

This model is useful for studying the bulk effect of rain on backscatter, because it combines three sources of uncertainty into two. Thus, the PR radiative transfer model in rainy conditions is given by

$$\sigma_{\text{wind}}^0 = \frac{1}{K}\left(\sigma_{\text{obs}}^0 - \sigma_{\text{eff}}^0\right), \tag{22}$$

where σ_{wind}^0 is the wind-only induced backscatter cross-section. The rain calibration model parameters of eq. (22) are calculated and related to integration rain rate for each

PR measurement and the rain attenuation K can be calculated by eq. (7). We model effective rain backscattering cross-section as four order polynomial of integration rain rate:

$$\sigma^0_{\text{eff}}(\theta) = \sum_{n=0}^{N} C_{\text{eff}}(n,\theta) R^n, \quad (23)$$

where $C_{\text{eff}}(n,\theta)$ are the polynomial coefficients shown in Table 1. As previously defined, R_{ir} is the integration rain rate. By using eqs. (7), (23) and (6), we can get the wind-induced backscattering cross-section σ^0_{wind} and retrieve ocean surface wind speeds accurately in rainy conditions.

In order to further analyze the effect of σ^0_{eff} on σ^0_{wind}, we introduce a new parameter $\Delta\sigma^0$ given by

$$\Delta\sigma^0 = \left\{10\cdot\log10\left(\sigma^0_{\text{wind}} - \sigma^0_{\text{eff}}\right)\right\} - \left\{10\cdot\log10\left(\sigma^0_{\text{wind}}\right)\right\}. \quad (24)$$

The rain intensity dependence of $\Delta\sigma^0$ for different incidence angles is shown in Figure 5. And x-coordinate and y-coordinate represent $\Delta\sigma^0$ and rain intensity respectively. As shown in Figure 5, $\Delta\sigma^0$ decreases monotonically with rain intensity for different incidence. That is partially because σ^0_{eff} is a combination of σ^0_r which increases the energy of radar signal and $-\sigma^0_{\text{surf}}\cdot K$ which decreases the energy of radar signal, and the effect of σ^0_r is much weaker than the effect of $-\sigma^0_{\text{surf}}\cdot K$. Additionally, this trend is increasing with incidence angles at the same integration rain rate. For example, the value of $\Delta\sigma^0$ within 0°–4° is about 3 dB when rain intensity equals 17 dB mm h^{-1}, but this value increases up to 15 dB within 15°–18°. It indicates that the effect of effective rain backscattering on PR echo power for low incidence is weaker than large incidence. The reason is that the dominantly scattering mechanism for PR is the quasi-specular scattering. And the incidence dependence of PR signal power shows a deceasing trend for both horizontal and vertical polarization. At the low incidence within 0°–4°, the effective rain backscattering cross-section is much smaller than the PR signal power, and the effect of effective rain backscattering is very small and can even be neglected. However, with the incidence increasing, the PR signal due to quasi-specular scattering decreases rapidly, and the effect of effective rain backscattering becomes strong. This is the same reason why the wind speed can be retrieved accurately by altimeters but the scatterometers.

Table 1 Coefficients of four order fits to parameter σ^0_{eff} versus R_{ir}

Incident angle	$C_{\text{eff}}(0)$	$C_{\text{eff}}(1)$	$C_{\text{eff}}(2)$	$C_{\text{eff}}(3)$	$C_{\text{eff}}(4)$
0°–4°	–0.15	–0.72	0.028	–0.00048	3.2×10^{-6}
5°–9°	–0.085	–0.49	0.021	–0.00041	3.2×10^{-6}
10°–14°	–0.025	–0.21	0.0096	–0.0002	1.6×10^{-6}
15°–18°	–0.023	0.0038	0.00039	-8.1×10^{-5}	6.7×10^{-7}

4.2 Model validation

To quantify the performance of our rain calibration algorithm, we select three typhoon cases from June to August in 2012 to verify the accuracy of this model. The PR observation orbit number, locations of typhoon eye, and observation time are shown in Table 2.

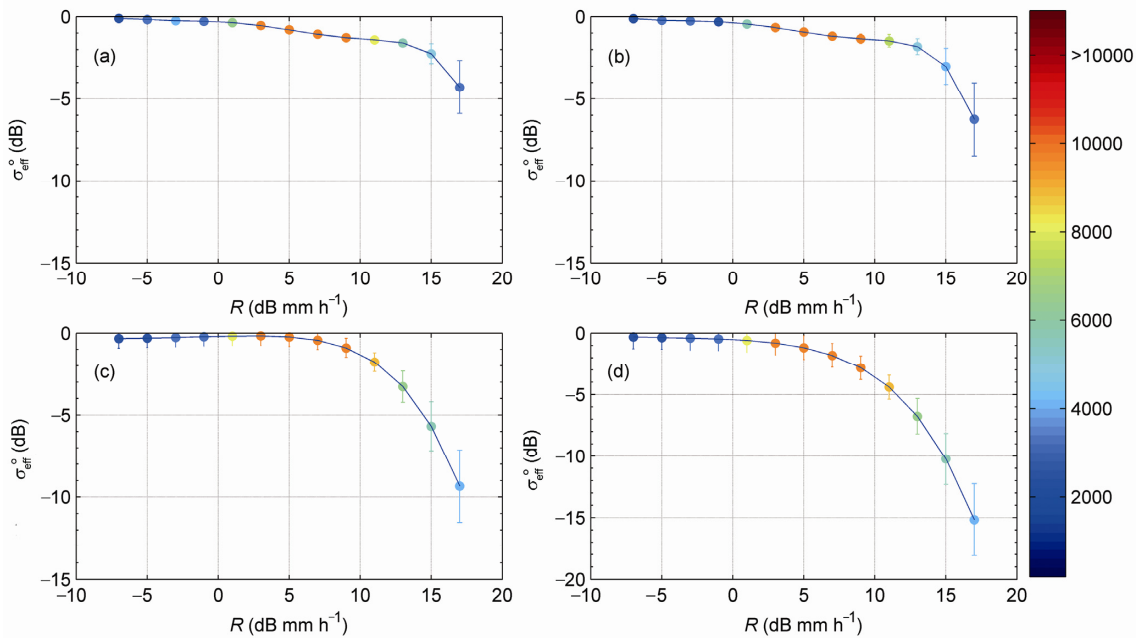

Figure 5 The rain intensity dependence of $\Delta\sigma^0$ for different incidence angles. (a) 0°–4°, (b) 5°–9°, (c) 10°–14°, (d) 15°–18°.

Figure 6 contains the information about the spatial distribution of PR-observed NRCS, NRCS after rain calibration, rain rate and match-up wind speed derived from TMI for typhoon Sandy which occurred in October 2012, and the number of PR orbit is 85170. And from the knowledge of the typical wind field structure of a mature typhoon, the wind direction of typhoon has a helical structure, and the wind speed on the eye-wall which is around the eye is much higher than the wind speed in the eye of typhoon which is always clear. Figure 6(a), (b) illustrates spatial distribution of rain rate and the TMI wind speed in the north of typhoon eye respectively, and the distance is about 100 km. The typhoon wind field data are obtained from the Hurricane Research Division (HRD). From the figure, we can see that the wind speed in the eye-wall with intense rain is higher than in other regions, and about half of PR-observed NRCS are corrupted by rainfall. Figure 6(a), (b) illustrates the spatial distribution of PR-observed NRCS before calibration and PR-observed NRCS after calibration. As previously analyzed, the effect of rain on PR-observed NRCS is to reduce the PR-observed NRCS whether at lower wind speeds or at higher wind speeds. From these pictures, we know that the PR-observed NRCS before calibration are smaller than after calibration. And this further proves the attenuation effect of rainfall on PR-observed NRCS.

Due to the effect of rain attenuation, PR-observed NRCS in rainy conditions are smaller than wind-only induced NRCS σ^0_{wind} apparently shown in Figure 7(a), and the mean difference and MSE are 2.95 and 3.18 dB respectively. However, this situation has been improved significantly after applying the rain calibration model to these measurements, and the mean difference and MSE are reduced to 0.64 and 1.61 dB respectively. It indicates that applications of this model to PR measurements in rainy conditions show a good agreement with the wind-only induced PR measurements and our model can be beneficial for PR wind speed retrieval in rainy conditions.

5 Summary

Rain can significantly degrade the wind vector retrieval from Precipitation Radar (PR) by three mechanisms, namely,

Table 2 The PR observation orbit number, locations of typhoon eye, and observation time

Typhoon name	Orbits	Location of typhoon eye	Observation time (UTC)
Debby	83204, 83205, 83206	86.0450°W, 16.8570°N	2012-06-24
	83219, 83222	85.4650°W, 28.6880°N	2012-06-25
Ernesto	83881, 83880	80.1650°W, 15.7360°N	2012-08-06
Sandy	85109	76.7340°W, 16.8570°N	2012-10-24
	85120	75.8000°W, 20.4750°N	2012-10-25
	85135, 85139	75.4630°W, 21.9980°N	2012-10-26
	85152, 85154	76.8130°W, 28.3110°N	2012-10-27
	85170	73.3230°W, 31.8710°N	2012-10-28

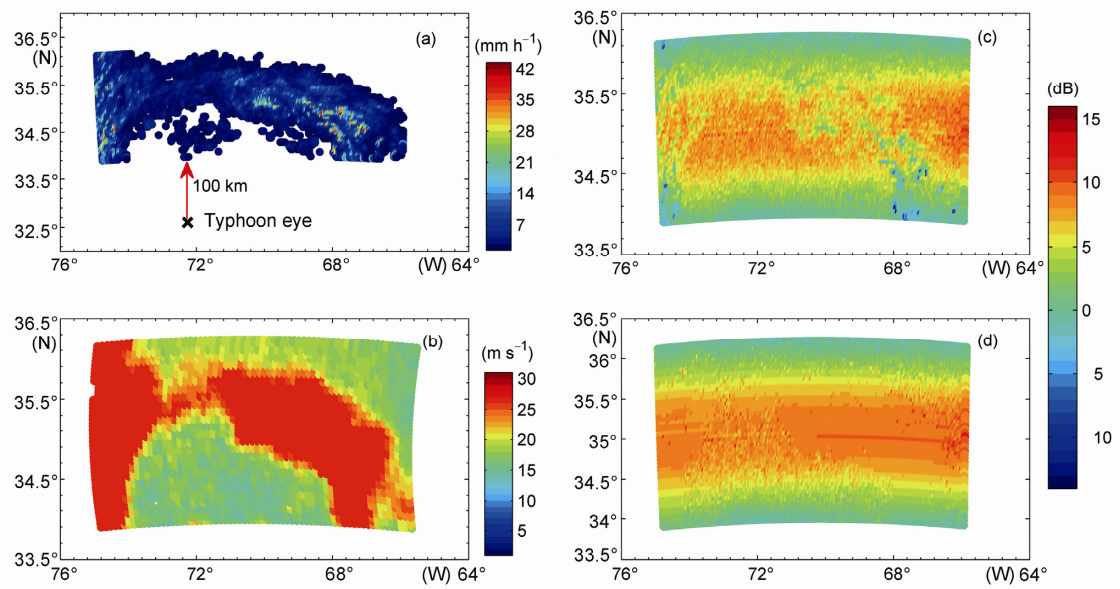

Figure 6 The spatial distribution of PR-observed NRCS, NRCS after rain calibration, rain rate and matchup wind speed derived from TMI for typhoon Sandy for orbit 85170. (a) Rain rate; (b)TMI wind speed; (c) PR-observed NRCS before calibration; (d) PR-observed NRCS after calibration.

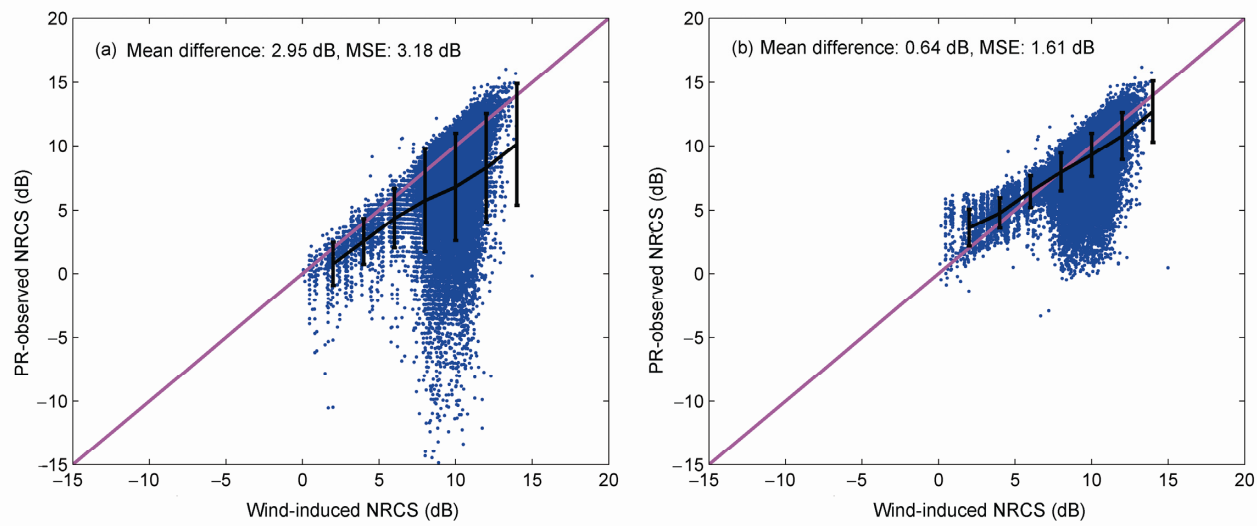

Figure 7 Comparison between PR-measured NRCS before rain calibration and PR-measured NRCS after rain calibration. (a) Before calibration; (b) after calibration.

two-way rain attenuation, rain volume-backscattering, and ocean surface roughening from the rain splash effect.

Based on the above three factors, we first derive the radar equation for PR in rainy condition. Then we use the rain attenuation model for Ku band, volume backscatter for spherical raindrops and PR-TMI (TRMM Microwave Imager, TMI) matchup datasets from June to August in 2010 to solve the radar equation, and quantitatively analyze the influence of rainfall on PR radar measurement of ocean surface wind speed. Our results show that the significant effect of rain on radar signal comes from the two-way rain attenuation that increases with rain rate and rain path, the splash effect which increases with rain rate and incident angle, and the effect of rain volume-backscattering is the relatively the weakest which can be neglected in rain-weak environments.

Lastly, we combine the volume-backscattering effect and the splash effect into a simple phenomenological model for rain calibration and select three typhoon cases from June to August in 2012 to verify the accuracy of this model. The results show that applications of this model to PR measurements in rainy conditions show a good agreement with the wind-only induced PR measurements and our model can be beneficial for PR wind speed retrieval in rainy conditions.

Existing space-borne active microwave sensors for tropical ocean observation include scatterometers, altimeters, and the PR. And the spatial and temporal resolution of PR measurement over tropical ocean is superior to scatterometers and altimeters. Therefore, our research can provide a theoretical basis for PR in typhoon-monitoring, and would be beneficial for expanding the business applications of PR over the Tropical Ocean. However, in this paper, we focused on the rain calibration algorithm for PR-observed NRCS, and did not mention the wind speed retrieval algorithm due to its complexity. The next stage is to apply our rain calibration model to the process of wind speed retrieval in rainy conditions, especially to typhoon monitoring.

We acknowledge helpful discussions with Xie Chao and Wang Anqi. This work was supported by National Natural Science Foundation of China (Grant No. 11101421), State Oceanic Administration (Grant No. Y1H0810034), and the Special Foundation for Young Scientists of Institute of Remote Sensing and Digital Earth, Chinese Academy of Sciences (Grant No. Y1S01500CX).

Bliven F L, Sobieski P, Craeye C.1997. Rain generated ring-waves: Measurements and modeling for remote sensing. Int J Remote Sens, 18: 221–228

Crane R K. 1971. Propagation phenomena affecting satellite communication systems operating in the centimeter and millimeter wavelength bands. Proc IEEE, 59: 173–188

Craeye C, Sobieski P W, Bliven F L. 1997. Scattering by artificial wind and rain roughed water surfaces at oblique incidences. Int J Remote Sens, 18: 2241–2246

Conner L N, Chang P S. 2000. Ocean surface wind retrievals using the TRMM microwave imager. IEEE Trans Geosci Remote Sensing, 38: 2009–2016

Chiu L S, Chang A T C. 2000. Oceanic rain column height derived from SSM/I. J Clim, 13: 4125: 4136

Durden S P, Vesecky J F. 1985. A physical radar cross-section model for a wind-driven sea with swell. IEEE J Oceanic Eng, 10: 445–451

Donneley W J, Carswell J R, McIntosh R E, et al. 1999. Revised ocean backscatter models at C and Ku-band under high wind conditions. J Geophys Res, 104: 11485–11497

David W D, David G L, 2004. Evaluating the effect of rain on sea winds scatterometer measurements. J Geophys Res, 109: C02005

Greent T, Houk D F, 1979. The mixing of rain with near-surface water. J Fluid Mech, 90: 569–588

Graf J, Sasaki C, Winn C, et al. 1998. NASA scatterometer experiment. Astron Astrophys, 43: 397–407

Kummerow C, Barnes W, Kozu T, et al. 1998. The Tropical Rainfall Measureing Mission (TRMM) sensor package. J Atmos Ocean Technol, 15: 809–817

Li Li, Eastwood I M, Stephen L, et al. 2001. A surface wind model-based method to estimate rain-induced radar path attenuation over ocean. J

Atmos Ocean Technol, 19: 658–672
Li Li, Im E, Connor L N, et al. 2004. Retrieving ocean surface wind speed from the TRMM precipitation radar measurement. IEEE Trans Geosci Remote Sensing, 42: 1271–1282
Laupattarakasem P, Jones L W, Hennon C C, et al. 2007. Improved hurricane ocean vector winds using seawinds Active/passive retrievals. IEEE Trans Geosci Remote Sensing, 48: 2909–2923
Manton M J. 1973. On the attenuation of sea waves by rain. Geophys Fluid Dyn, 5: 249–260
Meneghini R, Iguchi T, Kozu T, et al. 2000. Use of the surface reference technique for path attenuation estimates from the TRMM precipitation radar. J Appl Meteorol, 39: 2053–2070
Nystuen J A. 1989. A note on the attenuation of surface gravity waves by rainfall. J Geophys Res, 95: 18353–18355
Nielsen S N. 2007. A wind and rain backscatter model derieved from AMSR and Seawinds data. Master's Dissertation. Brigham: Brigham Yong University
Oguchi T. 1964. Attenuation of electromagnetic wave due to rain with distorted raindrops (part 2). J Radio Res Lab, 11: 19–44
Quilfen Y, Chapron B, Elfouhaily T, et al. 1998. Observation of tropical cyclones by high-resolution scatterometry. J Geophys Res, 103: 7767–7786
Poon Y K, Tang S, Wu J. 1992. Interactions between wind and waves. J Phys Oceanogr, 22: 976–987
Ray P S. 1972. Broadband complex refractive indices of ice and water. Appl Optics, 11: 1836–1844
Thurai M, Deguchi E, Okamoto K et al. 2005. Rain height variability in the tropics. Microwaves, Antennas and Propagation, Proc IEEE, 152: 17–23
Ulaby F T, Moore R K, Fung A K. 1981. Microwave Remote Sensing. Massachusetts: Addison-Wesley Publishing Company. 318–325
Yang Z, Tang S, Wu J. 1997. An experimental study of rain effects on fine structures of wind waves. J Phys Oceanogr, 27: 419–430
Yueh S H, Stiels B W, Tsai W Y, et al. 2001. QuikSCAT Geophysical Model Function for tropical cyclones and application to hurricane Floyd. IEEE Trans Geosci Remote Sensing, 39: 2601–2612
Yueh S H, Stiels B W, Liu W T, et al. 2003. QuikSCAT wind retrievals for tropical cyclones. IEEE Trans Geosci Remote Sensing, 2: 1250–1262
Lin H, Wei C, Lu D R. 1981. Microwave radiation characteristics of raindrop spectra. Sci Atoms Sin, 5: 188–197
Li Huang. 2007. Preliminary study on detecting atmospheric rainfall by rain attenuation from Ku-band satellite telecommunication system. J Remote Sens, 10: 568–572
Liu L, Li H, Gao T C. 2008. The approximate ellipsoid model for raindrop and its near-infrared scattering characteristics. Sci Meteorol Sin, 28: 271–275
Zhang L, Huang S X, Zhong J, Du H D. 2010. New GMF+RAIN model based on rain rate and application in typhoon wind retrieval. Acta Phys Sin, 59: 7478–7491
Shang J, Zhang P. 2009. Improvement research on radar reflectivity factor retrieval algorithm of space-borne precipitation radar. J Wuhan UnivTechnol, 31: 154–161
Zhang P C, Du B Y, Dai T P. 2000. Radar Meteorology. Section 2. Beijing: Meteorological Press. 70–73